CONTACT INTERACTIONS IN THE PROBLEM OF TOOTH CHAIN TRANSMISSION DYNAMICS

Yu. G. Ispolov
Physics and Mechanics Dept.
St. Petersburg State Polytechnical University
Russia
nym@online.ru

S. G. Orlov
Mechanical Engineering Dept.
St. Petersburg State Polytechnical University
Russia
majorsteve@mail.ru

Abstract
The problem of modeling the contact interactions in tooth chain transmission is considered. Chain plates are connected by pins consisting of two halves. Rolling of two rigid pin halves without slip is called normal. Contact forces are determined by deviation of actual rolling from normal one. Contact interaction between teeth of the chain and the sprockets takes place at contact points. Special algorithm for the determination of contact points is developed. The algorithm uses a tree-like search structure consisting of circles embedded within each other.

Key words
Multibody dynamics, nonlinear systems, contact interaction.

1 Problem formulation

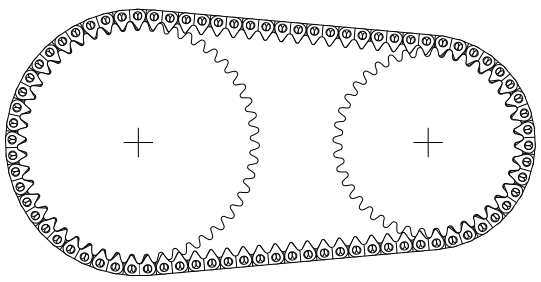

Figure 1. Tooth chain transmission model

The problem of modeling the contact interactions in tooth chain transmission (Fig. 1) is considered. The transmission consists of the tooth chain that connects two sprockets. The chain consists of tooth plates that are contacting the profiled teeth of the sprockets and are connected by the pins. Planar motion is considered.

The assembly of two plates connected with pins is shown in Fig. 2.

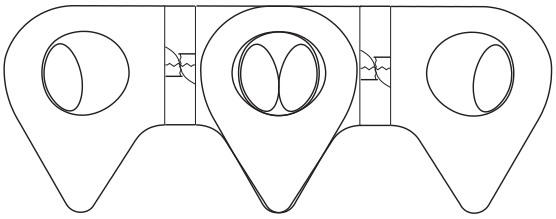

Figure 2. Schematic of tooth chain

The model of the tooth plate assumes that it consists of two halves that are absolutely rigid with an elastic connection. Each half has tooth profile that is designed to contact the sprockets. Chain plates are connected by pins consisting of two halves (see Fig. 2). When relative rotation appears between the contacting halves of the pins, they roll over each other. Sprockets have contact profiles to interact with the plates.

During interaction between the pin halves, as well as between the chain teeth and the sprockets' teeth, there develop normal and tangential contact forces. Description of the contact interactions in the framework of finite element approach leads to very large computation time. In the paper we discuss special approaches, which allows to significantly reduce the computation time.

2 Contact interaction between pin halves

The concept of "normal rolling" is introduced to denote rolling of rigid pin halves without slip. Fig. 3 shows the two rolling contours in the position on straight section of the chain.

Let the contours of the pin halves in the coordinate systems rigidly connected with these halves be determined by parametric equations $\boldsymbol{r}^- = \boldsymbol{r}^-(s)$ and $\boldsymbol{r}^+ = \boldsymbol{r}^+(s)$. Initial contact point that corresponds to

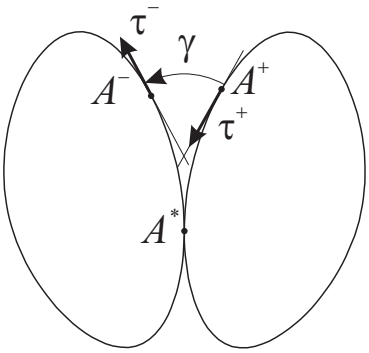

Figure 3. Geometry of normal rolling case for pin halves

the position of pins when the chain is straight is denoted A^*. When two rigid bodies roll over each other without slip, the distances calculated along the arcs of the contours from the initial contact point should be the same. When rolling without slip, the point A^+ will coincide with A^- after relative rotation of the two pin halves to angle γ. It makes it possible to find the values of parameters s^- and s^+ as the functions of γ: $s^- = s^-(\gamma)$, $s^+ = s^+(\gamma)$ and further obtain the values of radius-vectors of points A^- and A^+, $\boldsymbol{r}_{A^-} = \boldsymbol{r}_{A^-}(s^-(\gamma))$ and $\boldsymbol{r}_{A^+} = \boldsymbol{r}_{A^+}(s^+(\gamma))$, as well as the unit vectors of tangents and normal to the contours $\boldsymbol{\tau}^\pm = \boldsymbol{\tau}^\pm(s^\pm(\gamma))$, $\boldsymbol{n}^\pm = \boldsymbol{n}^\pm(s^\pm(\gamma))$ in coordinate systems attached to corresponding pin halves.

In the dynamic model the position of every pin half is determined by independent generalized coordinates and the geometry of rolling is different from normal rolling case. For real rolling there develops the deformation of the surfaces of pin halves and the forces pointing along their normal vectors that prevent penetration of one pin half into the other. Besides, when the pin halves slip with respect to each other, the friction forces develop pointing along the tangents to the contact surfaces to resist it.

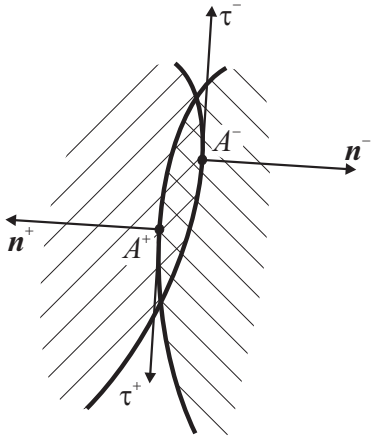

Figure 4. Position of contacting surfaces of pin halves

The position of contacting surfaces of pin halves in the framework of the developed model is presented in Fig. 4. The pin halves are shown penetrating each other (in reality, of course, this is not the penetration, but the deformation of the contact layer). Points A^- and A^+ in Fig. 4 are the points that are in contact in normal rolling case (for known angle γ of relative rotation between the pin halves). Vectors $\boldsymbol{\tau}^\pm$, $\boldsymbol{n}^\pm$ are the vectors of tangents and normals to the contours of pin halves in normal rolling case.

Further we assume that the value of elastic normal force at the contact surface is determined by the depth of "penetration" between the two pin halves:

$$\Delta_n = (\boldsymbol{r}_{A^-} - \boldsymbol{r}_{A^+}) \cdot \boldsymbol{n}^- \tag{1}$$

The elastic normal force $F^{n,e}$ that appears on the contact surface is estimated basing on the known solution of the problem of contact interaction between two circular cylinders with parallel axes. The formula that connects the magnitude of approach between the parallel axes of contacting cylinders, $\widetilde{\Delta}$, and the force acting on the unit length of the cylinder, q, for cylinders with the same Young's modulus, E, Poisson's ratio $\nu = 0.3$, takes the form [Birger and Panovko, 1968]:

$$\widetilde{\Delta} = 0.579\frac{q}{E}\left(\ln\frac{4R_1R_2}{b^2} + 0.814\right), \tag{2}$$

where R_1, R_2 are the radii of the cylinders, and

$$b = 1.522\sqrt{\frac{q}{E}\frac{R_1R_2}{R_1+R_2}} \tag{3}$$

is the width of the contact patch.

We use formula (2) assuming

$$\Delta_n = \widetilde{\Delta}, \qquad F^{n,e} = ql^{pin} \tag{4}$$

where l^{pin} is the pin length.

Except the elastic normal force $F^{n,e}$, the damping force acting along the normal vector also exists. The normal damping force, $F^{n,d}$, is proportional to the deformation rate $\dot{\Delta}_n$:

$$F^{n,d} = b^{n,d}\dot{\Delta}_n, \tag{5}$$

where $b^{n,d}$ — normal damping coefficient.

The friction force acting along the tangent, R^τ, is proportional to the normal elastic force $F^{n,e}$ and the friction coefficient f:

$$R^\tau = fF^{n,e}\,\mathrm{sign}(\dot{\Delta}_\tau). \tag{6}$$

where the friction coefficient f is a function of the absolute value of slip speed $\dot{\Delta}_\tau$: $f = f(|\dot{\Delta}_\tau|)$, $\Delta_\tau = (\boldsymbol{r}_{A^-} - \boldsymbol{r}_{A^+}) \cdot \boldsymbol{\tau}^-$.

3 Contact interaction of chain teeth and sprockets

In the model of contact interaction, the following assumptions are made. In motion, when the boundaries of the bodies intersect, the contact interaction occurs, that takes place in contact points, where forces are applied to contacting bodies.

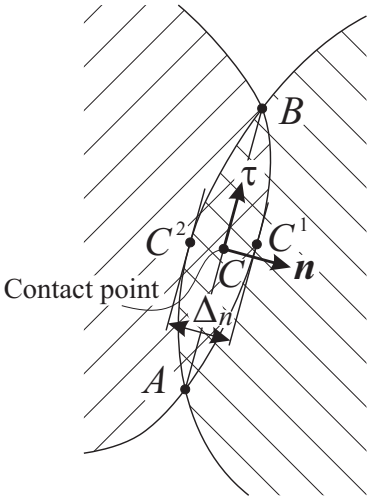

Figure 5. Local geometry of contact

Fig. 5 shows two bodies with boundaries intersecting at points A and B. We define the contact point, C, as the point lying in the middle between the points A and B: if the positions of A and B are respectively $\boldsymbol{r}_A$ and $\boldsymbol{r}_B$, then the position of point C, $\boldsymbol{r}_C$, is

$$\boldsymbol{r}_C = \frac{1}{2}(\boldsymbol{r}_A + \boldsymbol{r}_B). \tag{7}$$

The definitions of normal vector, $\boldsymbol{n}$, and tangent vector, $\boldsymbol{\tau}$, at contact point C also involve the positions of the intersection points A and B:

$$\boldsymbol{\tau} = \frac{\boldsymbol{r}_B - \boldsymbol{r}_A}{|\boldsymbol{r}_B - \boldsymbol{r}_A|}, \qquad \boldsymbol{n} = \boldsymbol{\tau} \times \boldsymbol{e}_3. \tag{8}$$

Contact deformation at point C, Δ_n, is defined as the distance between points C^1 and C^2 along the normal vector $\boldsymbol{n}$ (see Fig. 5):

$$\Delta_n = \boldsymbol{n} \cdot (\boldsymbol{r}_{C^1} - \boldsymbol{r}_{C^2}). \tag{9}$$

The points C^1 and C^2 lie in the middles of the arcs of the boundaries between the intersection points A and B.

Forces in the contact point are similar to the forces between pin halves. The normal force consists of elastic component $F^{n,e}$ (which can be calculated using formulas similar to (2–4)) and damping component $F^{n,d}$ (which can be calculated using formula similar to (5)). The tangential friction force R^τ is calculated using formula similar to (6) with the tangential speed at contact point, v_τ, defined as follows:

$$v_\tau = (\boldsymbol{v}_{C^1} - \boldsymbol{v}_{C^2}) \cdot \boldsymbol{\tau}, \tag{10}$$

where $\boldsymbol{v}_{C^1}$ and $\boldsymbol{v}_{C^2}$ are the speeds of points C^1 and C^2.

Finding intersection points of the boundaries of two bodies, they are approximated by polygons. For the adequate modeling of the geometry of teeth of the chain and the sprockets, the polygons have large number of vertices. Typically, the polygon approximating the outer boundary of a plate half has hundreds of vertices, and the polygon approximating the boundary of the sprocket has thousands of vertices. A straightforward algorithm for determination of intersection points would perform an intersection test for each pair of edges of two polygons; this would lead to 10^5–10^6 tests in our case, which is unacceptable due to the performance reasons. Special technique was implemented to find the intersection points efficiently, similar to the approach proposed in [Palmer and Grimsdale, 1995] for the 3D case.

The main idea of the proposed algorithm is to reduce the number of intersection tests. The polygons approximating the boundaries of the moving rigid bodies do not change their shapes. This allows building a static search structure for each of the polygons. The generation of the search structure takes the time $O(K \ln K)$, K being the number of vertices, and is only done once, at the beginning of simulation.

Suppose that the polygon has K vertices, $V_1, \ldots, V_K$, and K edges, $e_1, \ldots, e_K$ (first edge connects V_1 with V_2, i-th edge connects V_i with V_{i+1}, K-th edge connects V_K with V_1). The search structure consists of circles embedded within each other, and it is built as follows.

1. Generate the initial covering of all edges. The covering consists of circles, each covering a certain edge and having the diameter equal to edge length. The circles of the initial covering are denoted as $o_1^1, o_2^1, \ldots, o_{K_1}^1$ ($K_1 = K$), and their set — as O^1.
2. Set the covering counter, k, to 1.
3. Generate the $(k+1)$-th covering, O^{k+1}, that covers the k-th covering, O^k. The following rule is used: the i-th circle of the new covering, o_i^{k+1} must contain two circles of the previous covering, o_{2i-1}^k and o_{2i}^k: $o_i^{k+1} \supset o_{2i-1}^k \cup o_{2i}^k$. If K_k is even, then the new covering consists of $K_{k+1} = K_k/2$ circles, and each circle contains two circles from the previous covering. If K_k is odd, then everything is similar, but the last circle of the new covering contains three last circles of the previous covering and, thus, the new covering consists of $(K_k - 1)/2$ circles.
4. Increase k by one.

5. If $K_k > 1$, go to step 3, otherwise stop.

The search structure for the right link half is shown in fig. 6.

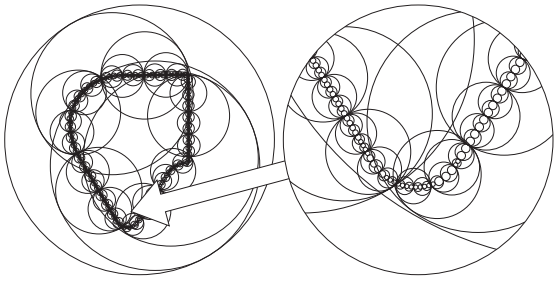

Figure 6. Search structure for the link half contour

Once the search structures described above are built for each of the contacting bodies, a very simple and time-efficient algorithm can be proposed to find intersection points of the polygons' boundaries. To describe the algorithm, let's introduce additional superscript that denotes the body number and takes the values 1, 2: further we write $o_i^{k,\alpha}$ instead of o_i^k, V_i^α instead of V_i and so on. Let M^1 and M^2 be the numbers of coverings in the search structures for the boundaries of two contacting bodies, Γ^1 and Γ^2. The algorithm performs the recursive intersection test for the circles $o_1^{M_1,1}$ and $o_1^{M_2,2}$. The test verifies whether given circles, $o_i^{m_1,1}$ and $o_j^{m_2,2}$ intersect or not. If the circles don't intersect, the test finishes indicating that no intersection occurs inside the given circles. If the circles do intersect, the test verifies if m_1 and m_2 are both equal to 1. If so (we are testing two circles of the initial coverings), the corresponding edges of Γ^1 and Γ^2 are tested for intersection. If the edges intersect, the intersection point is stored; if not, nothing happens; then the test returns. Otherwise, if either m_1 or m_2 is greater than one, if $m_1 = 1$, the test calls itself recursively for $o_i^{m_1,1}$ and all circles $o_k^{m_2-1,2} \in o_j^{m_2,2}$, and then returns. Otherwise ($m_1 > 1$), if $m_2 = 1$, the test calls itself recursively for all circles $o_k^{m_1-1,1} \in o_i^{m_1,1}$ and $o_j^{m_2,2}$, and then returns. Otherwise, if both m_1 and m_2 are greater than one, the test compares $R_i^{m_1,1}$ and $R_j^{m_2,2}$, the radii of the circles $o_i^{m_1,1}$ and $o_j^{m_2,2}$. If $R_i^{m_1,1} / R_j^{m_2,2} > 1.5$, then the test calls itself recursively for all circles $o_k^{m_1-1,1} \in o_i^{m_1,1}$ and $o_j^{m_2,2}$, and then returns. Otherwise, if $R_i^{m_1,1} / R_j^{m_2,2} < 1/1.5$, then the test calls itself recursively for $o_i^{m_1,1}$ and all circles $o_k^{m_2-1,2} \in o_j^{m_2,2}$, and then returns. Otherwise the test calls itself recursively for all pairs $(o_k^{m_1-1,1}, o_p^{m_2-1,2})$, where $o_k^{m_1-1,1} \in o_i^{m_1,1}$, $o_p^{m_2-1,2} \in o_j^{m_2,2}$, and then returns.

The presented algorithm is very efficient compared to the straight-forward one: over the whole chain at certain time instant, the average number of tests required to find intersections of the link half with the sprocket we have found is 73.6, among which 62.4 are simple tests (intersection of two circles) and 11.2 are complex tests (intersection of two edges). Maximum number of simple tests is 266; maximum number of complex tests is 60. The efficiency compared to the straightforward algorithm is significantly better, because the latter would always do about 10^6 complex tests. However, our algorithm admits further optimization.

4 Numerical experiments

To verify the models of contact interactions the differential equations of motion for tooth chain transmission were obtained in Lagrange form and numerical integration of these equations was carried out. Below we give the results of numerical experiments in one of stationary regimes.

The parameters of the regime are as follows: input torque, $M_1 = 3$ KN; angular speed of driving sprocket, $\omega_1 = 600$ rpm; angular speed of driven sprocket, $\omega_2 = 750$ rpm; gear ratio $i = 39/49 \approx 0.796$.

Plots of the values of normal forces that develop between the pin halves are presented in Fig. 7.

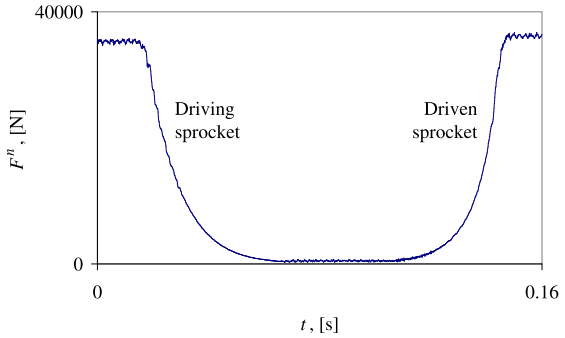

Figure 7. Normal contact force between the pin halves, for one chain cycle

Plots of the values of normal forces that develop between the teeth of the chain and the sprockets are presented in Fig. 8, 9.

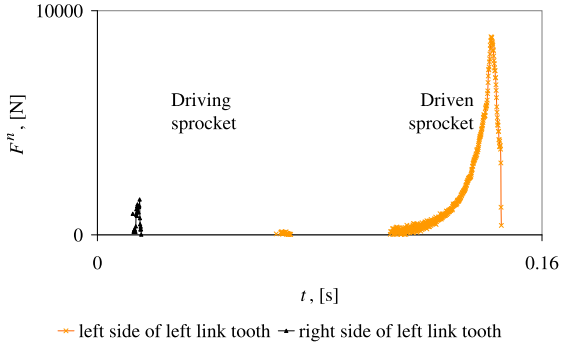

Figure 8. Normal contact forces between the left tooth of chain link and the sprockets, for one chain cycle

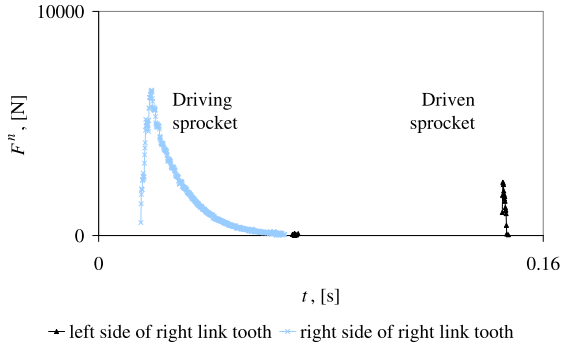

Figure 9. Normal contact forces between the right tooth of chain link and the sprockets, for one chain cycle

Fig. 8, 9 show that contact forces appear primarily between the left side of left link tooth and the driven sprocket, and between the right side of right link tooth and the driving sprocket.

The results of numerical experiments confirm the validity of the proposed models of contact interactions.

References

Strength, buckling, vibration. Reference book in three volumes. Vol. 2. Edited by Birger I. A. and Panovko Ya. G. Moscow, 1968. (In Russian)

I. J. Palmer and R. L. Grimsdale. *Collision Detection for Animation Using Sphere-Tree.* Computer Graphics Forum, 14(2), pp. 105–116, June 1995.